

Frequency stabilization and tuning of breathing soliton in SiN microresonators

Shuai Wan^{1,3}, Rui Niu^{1,3}, Zheng-Yu Wang^{1,3}, Jin-Lan Peng², Ming Li^{1,3},
Jin Li^{1,3}, Guang-Can Guo^{1,3}, Chang-Ling Zou^{1,3,*} and Chun-Hua Dong^{1,3†}

¹CAS Key Laboratory of Quantum Information, University of Science
and Technology of China, Hefei, Anhui 230026, P. R. China.

²Center for Micro and Nanoscale Research and Fabrication, University of Science and Technology of China,
Chinese Academy of Sciences, Hefei 230026, P. R. China. and

³CAS Center For Excellence in Quantum Information and Quantum Physics,
University of Science and Technology of China, Hefei, Anhui 230026, P. R. China.

Dissipative Kerr soliton offers broadband coherent and low-noise frequency comb and stable temporal pulse train, having shown great potential applications in spectroscopy, communications, and metrology. Breathing soliton is a particular dissipative Kerr soliton that the pulse duration and peak intensity show periodic oscillation. However, the noise and stability of the breathing soliton is still remaining unexplored, which would be the main obstacle for future applications of breathing solitons. Here, we have investigated the breathing dissipative Kerr solitons in the silicon nitride (SiN) microrings, while the breather period shows uncertainties around MHz in both simulation and experiments. By applying a modulated pump, the breathing frequency can be injectively locked to the modulation and tuned over tens of MHz with frequency noise significantly suppressed. Our demonstration offers an alternative knob for the controlling of soliton dynamics in microresonator and paves a new avenue towards practical applications of breathing soliton.

I. INTRODUCTION

Optical solitons which maintain their localized structures during propagation can be generated by balancing dispersion and nonlinearity in the propagation media [1, 2]. This phenomenon was firstly demonstrated in optical fiber, aiming to transmit information with increased bandwidth [3]. Since then, this kind of localized pulses has been explored and realized in various nonlinear systems and enables a variety of scientific and technological applications [4–8]. Whispering gallery mode (WGM) microresonators, hold the advantages of high optical quality factor (Q-factor) and the small mode volume [9], could greatly enhance light-matter interaction and thus provide an alternative platform for studying these fascinating nonlinear physics [5, 6, 11, 13]. In addition, the microresonator in the integrated photonic platform is excellent for future applications with high stability, reduced size and costs.

The first observation of optical microcomb was realized in 2007 [10] and after several years of deep studies in overcoming challenges of low coherence, optical soliton was successfully generated in a crystalline microresonator [11]. Compared to the aforementioned soliton generation schemes, in addition to the balance of dispersion and nonlinearity, soliton generation in WGM microresonators also requires the balance of loss and gain. Such optical soliton is called dissipative Kerr soliton (DKS) and firstly observed in the mode-locked fiber laser [12]. Different from the mode-locked fiber laser, where the gain

is from an active media, the gain in the passive WGM microresonator is the parametric gain of four-wave mixing (FWM) stimulated by an external continuous-wave (CW) laser. The rapid development of DKS in microresonators makes it quite a good candidate for applications in ultra-high data rate communication [14], quantum key distribution [15], high precision optical ranging [16], dual-comb spectroscopy [17, 18], low-noise microwave source [19], optical clock [20] and astronomical spectrometer calibration [21, 22].

Associate with DKS, a series of novel nonlinear phenomena have been observed, such as dark pulses, Cherenkov radiation, Raman self-frequency shift, and breathing soliton. In particular, breathing solitons exhibit periodic oscillation behavior in both amplitude and pulse duration, which is related to the Fermi-Pasta-Ulam recurrence [24]. It has drawn a lot of attentions for fundamental studies of nonlinear physics and was demonstrated in experiments recently [24–28]. It is revealed that breather soliton state could exist in the detuning region between modulation instability state and stable DKS state because of intrinsic dynamical instability [24–26] or in the conventionally stationary DKS region because of the intermode interaction like avoided mode crossing [27]. Furthermore, in addition to bright breather solitons, dark breather solitons have also been observed in normal dispersion microresonators [28]. However, in the aforementioned studies, only the basic features of the breathing behavior are reported, and the breathing soliton is treated as unwanted because of the degradation of soliton stability. Therefore, the stability or noise properties of the breather soliton are not carefully studied, and the potential applications of the breath soliton are still remaining unexplored.

In this work, we demonstrate the stabilization and con-

*Electronic address: clzou321@ustc.edu.cn

†Electronic address: chunhua@ustc.edu.cn

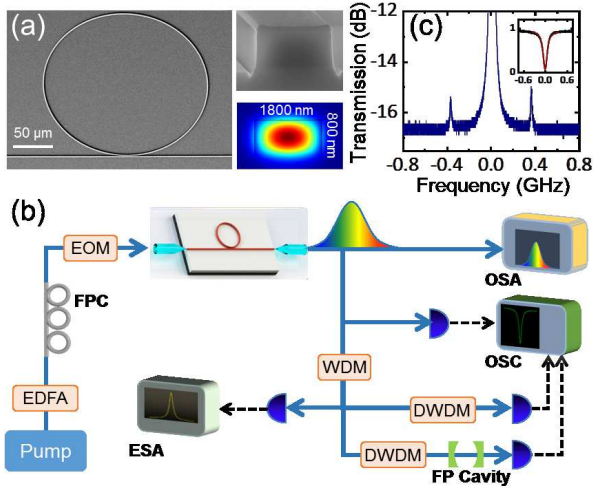


FIG. 1: (a) Scanning electron micrographs of Si_3N_4 microring with diameter of $200\ \mu\text{m}$. Insets show the microring cross-section of $1.8\ \mu\text{m} \times 0.8\ \mu\text{m}$ and the corresponding fundamental transverse-magnetic mode profile. (b) The experimental setup for Kerr frequency comb generation. EDFA, FPC, EOM, WDM, DWDM, FP, OSC, and ESA are erbium-doped fiber amplifier, fiber polarization controller, electro-optical modulator, wavelength division multiplexing, dense wavelength division multiplexing, Fabry-Perot cavity, oscilloscope and electronic spectrum analyzer, respectively. (c) Detailed comb line spectrum of a breathing microsoliton measured by the FP spectrum analyzer, with two sidebands indicating the breathing frequency around 0.4 GHz. The inset shows a typical resonance of the microring, with a loaded Q of 1.5×10^6 according to the Lorentzian fitting (red line).

trolling of the breathing frequency of microsoliton, for the first time among all platforms, via injection locking. Through both numerical and experimental studies, we demonstrate that the breathing frequency can be injection-locked by applying an appropriate modulation signal to pump laser, and then the phase noise of the system is remarkably suppressed. Furthermore, the stabilized breathing frequency is tuned over 50 MHz. Our approach to stabilize and control the breathing frequency paves the way towards the applications of the breathing soliton. For example, the breathing soliton provides a robust way to transfer RF frequencies between very different optical frequency lines through broadband microsoliton. Additionally, our demonstration also provides a convenient approach to study the differential absorption spectra, by comparing the sidebands of each comb line due to the locked breathing frequency modulation.

II. DEVICE FABRICATION AND SETUP OF SOLITON GENERATION

In our experiment, Si_3N_4 integrated microring resonator is fabricated with a diameter of $200\ \mu\text{m}$ and a cross-section of $1.8\ \mu\text{m} \times 0.8\ \mu\text{m}$, which is designed for the anomalous group velocity dispersion that required

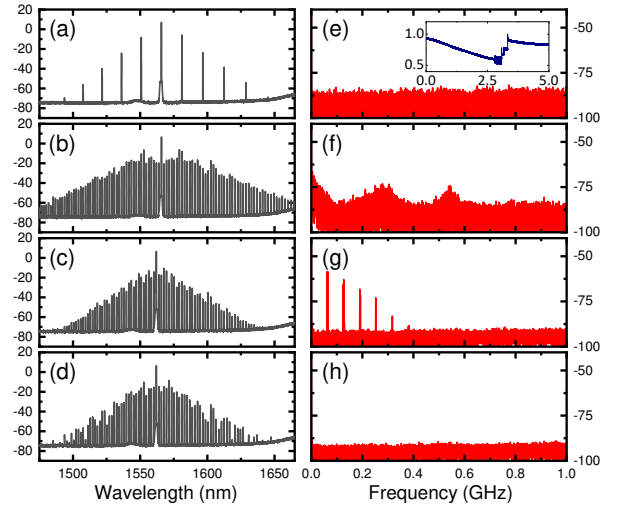


FIG. 2: The evolution of the microsoliton generation processes during the scanning of the pump laser detuning. (a-d) Typical optical spectra. Four evolution stages are primary comb (a), modulation instability comb (b), breather soliton (c) and stable soliton (d), respectively. (e-h) The corresponding evolution of RF spectra. Inset: The transmission spectrum of the microring when the laser frequency is scanning across the resonance mode.

for frequency comb generation. Figure 1(a) shows the scanning electron microscopy (SEM) photon of a typical device, which consists of a microring and a straight bus waveguide. The SEM of the microring cross-section before removing the residual photoresist is shown in the upper right inset, with the corresponding fundamental optical mode profile shown in the bottom inset. The devices are fabricated from a silicon substrate wafer with $500\ \mu\text{m}$ silicon, $3\ \mu\text{m}$ wet oxidation silicon dioxide (SiO_2) and $800\ \text{nm}$ deposited stoichiometric Si_3N_4 . To prevent cracks by high tensile stress of the Si_3N_4 film, some trenches are created around the wafer by a diamond scribe before the deposition [29]. A series of optimization techniques are also performed during the fabrication processing and finally, an upper cladding of $3\ \mu\text{m}$ SiO_2 is deposited by using plasma-enhanced chemical vapor deposition (PECVD) to cover the sample. More details about the fabrication process are provided in the Supporting Information. Then, the devices are tested by the setup shown in Fig. 1(b). A tunable CW laser (Toptica CTL 1550) is coupled into and out of the chip through lensed fibers. The coupling loss of lensed fibers is measured to be $\sim 3.5\ \text{dB}$ at each facet. In the inset of Fig. 1(c), a typical transmission spectrum of a fundamental mode is shown and fitted by a loaded Q -factor of $\sim 1.5 \times 10^6$. The high extinction ratio of the resonance indicates a high intrinsic Q -factor of 3×10^6 and high efficiency energy delivering from the bus waveguide to the modes, both are beneficial for nonlinear optics effects.

Soliton generation is achieved by sweeping the pump laser frequency over a resonance mode with higher power of 100 mW, from the blue-detuned regime to the red-

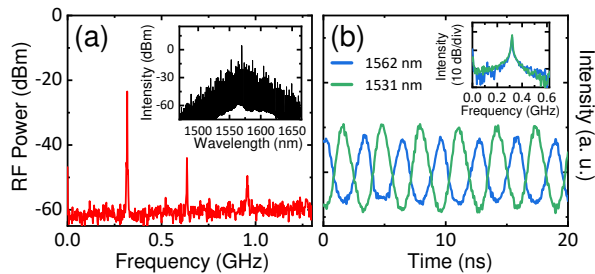


FIG. 3: Features of breathing soliton. (a) The detailed RF spectrum of a breather soliton state. Inset: the corresponding optical spectrum. (b) The recorded fast power evolution of a single comb line around the center (1562 nm, blue curve) and in the wings (1531 nm, green curve) of breather optical spectrum, respectively. Inset: the corresponding Fourier transform spectrum.

detuned regime [1, 13, 14, 18]. During the laser frequency scanning, the cavity fields build up, and strong nonlinear four-wave mixing effect induces the comb generation and essentially realizes the soliton. A complete spectral evolution can be divided into four stages, including primary comb, modulation instability (MI) comb, breather soliton, and stable soliton, as shown by the optical spectra and radio frequency (RF) spectra in Fig. 2. The inset is the corresponding transmission spectrum when scanning the pump. By carefully monitoring the transmitted power and stopping the pump frequency scanning at a certain detuning point, the four stages could be repetitively accessed in experiment.

III. RESULTS AND DISCUSSIONS

A. Breathing soliton

Among the four stages of the comb evolution, we are particularly interested in the breathing soliton. We verified the generation of breathing solitons in different devices with varying pump conditions. Figure 1(c) shows the optical spectrum measured by a Fabry-Perot cavity spectrometer. Two sidebands are obvious around the comb line, showing a breathing frequency f_{br} of about 380 MHz. In another device, we studied the RF spectrum and temporal oscillation of individual comb lines, as shown in Fig. 3. From the RF spectrum, we can find that the breathing frequency around 320 MHz. Then, the dense wavelength division multiplexing (DWDM) is used to filter out the single comb line around the center (~ 1562 nm) and the wings (~ 1531 nm), which is detected by a fast photodetector (PD) and recorded by an oscilloscope, as shown in Fig. 3(b). Here, we record the traces over 200 ns and compute the RF spectrum based on the Fourier transform. As shown in the inset of Fig. 3(b), the oscillation frequency is same as the frequency shown in Fig. 3(a). And the traces of the two comb lines are nearly out-of-phase when compared with each other, re-

vealing that there exists a periodic energy exchange between comb lines around the center and the wings, which is a characteristic of Fermi-Pasta-Ulam recurrence and a typical signature of breather solitons.

Comparing the breathing solitons in different experiments, we found that the breathing behavior could be robustly obtained in our devices, while its frequency varies from device to device. Even for a single device, the breathing frequency is not fixed. Here, we observe that the linewidth of the RF beatnote is on the order of megahertz, indicating a fast drifting of the breathing frequency. In the time traces, the fluctuations are obvious even in 10 ns time-scale. Therefore, the problems of the inhomogeneous breathing frequencies and the frequency instability hinder the potential applications of the breathing soliton.

B. Scheme of injection-locking

The stabilization and controlling of breathing frequency is of great significance, because it is not only helpful for a better understanding of nonlinear dynamics in microresonators, but also critical for many potential

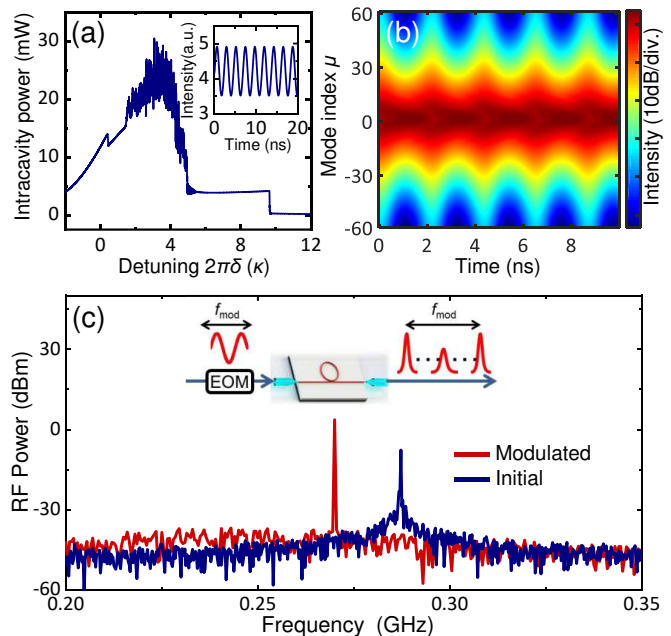


FIG. 4: (a) The simulated evolution of the intracavity power when the laser frequency is scanning across the resonance mode. The inset shows the oscillations of the power for a fixed laser frequency in the breather soliton state. (b) Periodic spectrum evolution of a breather soliton state. (c) RF spectra of initial breather soliton state (blue line) and modulated breather soliton state (red line). The initial breathing frequency f_{br} is 287 MHz and the modulated frequency f_{mod} is 270 MHz. Inset shows the concept of injection locking of breather soliton. A modulation signal with f_{mod} is applied to the pump laser after the appearance of breather soliton and f_{br} is injection locked if f_{mod} is within the locking range.

applications. Here, we envision two intriguing application scenarios enabled by the breathing soliton. First, we could use a single breather soliton, instead of two microresonators in the dual-comb scheme, for applications in spectroscopy. As can be noted from Fig. 1c, with the occurrence of the breather soliton, a series of sidebands can be observed around each comb line. Compared with the mode spacing of each comb line, these sidebands have much smaller frequency separation, which is equal to the breathing frequency. Therefore, the generated sidebands can provide additional differential absorption spectra around each comb line and an enhanced local resolution is expected. Second, the breathing could transfer a sub-GHz signal among all comb lines that would span an octave of wavelength. Thus, the breathing soliton could be used for distributing RF frequency references.

However, from our experiments, the breathing frequency depends on many practical parameters, such as the pump power, pump detuning, temperature of the chip, the polarization in the fiber and the coupling between the fiber lens and the chip. It is almost impossible to suppress all these imperfections in the experiments. Therefore, we propose to lock the breathing frequency by an external injection of RF signal, as illustrated in the inset of Fig. 4(c). An intensity electro-optic modulator (EOM) was introduced to modulate the pump power with an appropriate modulation signal. The frequency sidebands generated by the modulator could stimulate the four-wave mixing in a single mode and expand mode to mode during soliton generation. This stimulated process competes with the natural oscillation induced by spontaneous four-wave mixing in breather soliton. We expect it dominates the sidebands generation with strong enough modulation depth, the wide oscillation spectrum caused by spontaneous process and environment fluctuation be suppressed.

In order to investigate the feasibility of this approach, the numerical simulation is performed based on the coupled-mode equations (CME) [30–32]. First of all, we numerically test the stages of frequency comb generation with fixed pump power of 100 mW. The simulation parameters of the microring are the same as the device used in our experiments. Figure 4a shows the simulated evolution of the intracavity power when scanning the pump frequency. For more details about the numerical model, see Supplementary materials. In good agreement with our experiments [Fig. 2], there are clearly four states as the laser is tuning across the resonance mode [6]. By stopping the laser frequency on the breather soliton stage, it can be observed that the intracavity power experiences the periodic oscillation, as shown in the inset of Fig. 4(a). A spectral envelope evolution of the breather soliton is also depicted in Fig. 4(b), which shows the power of the breather soliton flows to the wings of the spectrum and returns to the center periodically, agrees with Fig. 3(b). Then, the injection locking scheme is numerically investigated by applying a modulation signal on the pump power with a modulation frequency f_{mod} ,

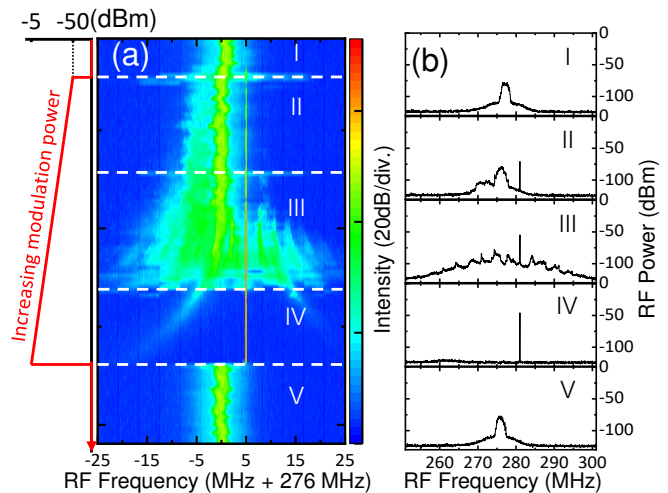


FIG. 5: (a) Evolution of the RF spectrum when gradually increasing the modulation power from -50dBm to -5dBm. The initial breathing frequency f_{br} is 276 MHz (I) and the modulation frequency f_{mod} is 281 MHz. With the increase of the modulation power, there is a competition between f_{br} and f_{mod} and other harmonics components appears (II and III). Eventually, f_{br} is synchronized to f_{mod} as the modulation power is strong enough (IV). f_{br} returns back to the initial frequency after turning off the modulation signal (V). (b) Snapshots with different evolution stages in (a).

which is close to f_{br} . Figure 4(c) shows the RF spectra for the breathing soliton with and without injection-locking. It is found that the breathing frequency is locked to the $f_{mod} = 270$ MHz (red line) even it is about 17 MHz away from its natural breathing frequency (~ 287 MHz, blue line). In addition, the RF noise background is suppressed by the injection locking, and the linewidth of the beatnote is much narrower than without injection locking.

C. Stabilization of breathing frequency

With the scheme validated numerically, we performed the injection locking for the breathing frequency stabilization. In our experiment, we use a sinusoidal wave signal to drive the EOM and monitor the evolution of the RF spectrum around the initial f_{br} when the modulation power varies from -50 dBm to -5 dBm with frequency of 281 MHz. The experimental results are summarized in Fig. 5. Before we turn on the modulator, a breather soliton state was generated at a f_{br} of 276 MHz and the linewidth of the beatnote on the RF spectrum is relatively wide (stage I). When we input the modulation signal and gradually increase the modulation power, as shown in Fig. 5a (stage II), a sharp peak at f_{mod} appears in the RF spectrum and the intensity of the f_{br} beatnote becomes weak, indicating that there exists a competition between this two frequencies and they can coexist when the modulation power is not strong enough. With further increasing the modulation power, f_{mod} gradually

gains the upper hand in the competition and multiple harmonics components arising from f_{mod} and f_{br} can be observed in the RF spectrum, which raises the noise of the background (stage III) along with the weak f_{br} beatnote. Eventually, as the modulation power is sufficiently strong, both the beatnote of f_{br} and other harmonics components vanish in the RF spectrum and only a beatnote of f_{mod} with narrow linewidth exists (stage IV). According to the recorded out-of-phase oscillatory power traces of comb lines around the center and in the wings at this stage, we can confirm that the breather soliton state still remains and f_{br} is synchronized to f_{mod} . Finally, we turn off the modulation signal and f_{br} immediately returns to the initial f_{br} and the linewidth became as wide as before (stage V). Since our experiment performs with a free-running pump laser without any stabilization scheme and f_{br} is sensitive to the pump power and effective detuning of the pump laser, as shown in Fig. 5, the initial f_{br} has obvious fluctuation and a slow red-drift before disappearing in the RF spectrum. Nevertheless, once f_{br} is injection-locked by f_{mod} , even pumped with a free-running laser, no fluctuation and drift are observed in the RF spectrum. In other words, the breather soliton with locked frequency is robust with unstable pump condition and the phase noise of the system is remarkably suppressed much narrower linewidth of f_{br} beatnote.

D. Controlling of breathing frequency

Furthermore, we study the locking range of this injection locking scheme. f_{mod} , which is scanned around the initial f_{br} , is applied on the pump laser with modulation power of 0.1 mW. Figure 6a shows the evolution of the RF spectrum centered at 262 MHz as we slowly vary f_{mod} . In the beginning, when the frequency difference Δf between f_{mod} and initial f_{br} is relatively large, beatnotes of initial f_{br} and f_{mod} and their harmonics components all exist in the RF spectrum. By continuing the scanning, when Δf is less than ~ 15 MHz, beatnote of initial f_{br} and harmonics components are eliminated, corresponding to the injection locking of f_{br} . Scanning in the same direction further leads to f_{mod} across the initial f_{br} and out of the locking range at last. We find that after scanning out of the range, the unlocked f_{br} drifts to a lower frequency of about ~ 5 MHz, which can be attributed to frequency red-drift of free-running pump laser during our measurement.

For the purpose of exploring the locking range as a function of modulation power, the above measurement of locking range is repeated with varied modulation power and obtained results are depicted in Fig. 6b. With the increase of the modulation power, the locking range rises rapidly at the very beginning and then this trend tends to slow down when the modulation power is beyond 0.2 mW. In our experiment, the maximum value of modulation power allowing the existence of a breather soliton state is 1 mW and the corresponding locking range

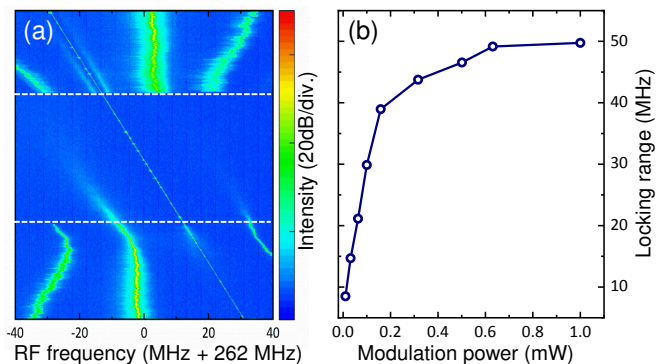


FIG. 6: (a) The evolution of the RF spectrum centered at 262 MHz with varied f_{mod} . The modulation power is 0.1 mW and f_{br} is synchronized to f_{mod} when the frequency difference Δf is less than ~ 15 MHz. (b) Locking ranges with varied modulation power.

is 50 MHz. In the case of modulation power greater than 1 mW, the breather soliton is annihilated. We attribute this observation to the excessively strong oscillation amplitude of the intracavity field induced by a strong modulation signal, which breaks the condition of the existence of breather soliton inside the microresonator. This phenomenon indicates that the modulation power exists an upper limit for effective injection locking.

IV. CONCLUSION

In conclusion, we have experimentally demonstrated the stabilization and tuning of breathing soliton via injection locking in high-Q Si_3N_4 microring. By applying an appropriate external modulation signal to the pump power, the breathing frequency can be effectively locked to the modulation frequency. Both frequency fluctuation and long term drift disappear even with a free-running pump laser, showing the high stability of the sub-GHz breathing frequency. Besides, the linewidth of breathing frequency beatnote is also become obviously narrower, indicating the apparent suppression of system phase noise. Being proportional to the modulation power, the locking range is able to reach ~ 50 MHz in our experiment. Therefore, a tunable and stable breathing frequency can be realized by using an EOM or other kinds of modulation instruments with no need for other feedback stabilization technique. The mechanism of injection-locking not only is universal for DKS in other material and structures, but also can be extended to stabilize oscillations in other nonlinear systems. In addition to the interesting nonlinear physics underlying the soliton and injection locking, our demonstration provides a robust way to transfer RF frequencies to broadband optical frequencies and a potential application in spectroscopy by utilizing the breathing sidebands to extract the high order spectral information around each comb line and boost the spectral resolution.

Experimental section

Methods and any associated references are mentioned in the Supporting Information.

Supporting Information

Supporting Information is available from the Wiley Online Library or from the author.

Acknowledgement 1 *S. Wan and R. Niu contribute*

equally to this work. The work was supported by the National Key R&D Program of China (Grant No.2016YFA0301303), the National Natural Science Foundation of China (Grant No.11934012 and 11722436), Anhui Initiative in Quantum Information Technologies (AHY130200), the Fundamental Research Funds for the Central Universities. This work was partially carried out at the USTC Center for Micro and Nanoscale Research and Fabrication.

-
- [1] P. Trocha, M. Karpov, D. Ganin, M. H. P. Pfeifer, A. Kordts, S. Wolf, J. Krockenberger, P. Marin-Palomo, C. Weimann, S. Randel, W. Freude, T. J. Kippenberg, and C. Koos, "Ultrafast optical ranging using microresonator soliton frequency combs," *Science* **359**, 887–891 (2018).
- [2] N. Akhmediev, and A. Ankiewicz, "Dissipative Solitons: From Optics to Biology and Medicine," (Springer, 2008).
- [3] S. Wabnitz, "Suppression of interactions in a phase-locked soliton optical memory," *Opt. Lett.* **18**, 601–603 (1993).
- [4] F. Leo, S. Coen, P. Kockaert, S.-P. Gorza, P. Emplit, and M. Haelterman, "Temporal cavity solitons in one-dimensional Kerr media as bits in an all-optical buffer," *Nat. Photonics* **4**, 471–476 (2010).
- [5] X. Yi, Q.-F. Yang, K. Y. Yang, M.-G. Suh, and K. J. Vahala, "Soliton frequency comb at microwave rates in a high-Q silica microresonator," *Optica* **2**, 1078–1085 (2015).
- [6] V. Brasch, M. Geiselmann, T. Herr, G. Lihachev, M. H. P. Pfeiffer, M. L. Gorodetsky, and T. J. Kippenberg, "Photonic chip-based optical frequency comb using soliton Cherenkov radiation," *Science* **351**, 357–360 (2016).
- [7] X. Xue, X. Zheng, and B. Zhou, "Super-efficient temporal solitons in mutually coupled optical cavities," *Nature Photonics* **13**, 616–622 (2019).
- [8] J. Peng, S. Boscolo, Z. Zhao, and H. Zeng, "Breathing dissipative solitons in mode-locked fiber lasers," *Science Advances* **5**, eaax1110 (2019).
- [9] K. J. Vahala, "Optical microcavities," *Nature* **424**, 839–846 (2003).
- [10] P. Del'Haye et al., Optical frequency comb generation from a monolithic microresonator. *Nature* **450**, 1214–1217 (2007).
- [11] T. Herr, V. Brasch, J. D. Jost, C. Y. Wang, N. M. Kondratiev, M. L. Gorodetsky, T. J. Kippenberg, "Temporal solitons in optical microresonators," *Nat. Photonics* **8**, 145–152 (2014).
- [12] P. Grellu, N. Akhmediev, Dissipative solitons for mode-locked lasers. *Nat. Photonics* **6**, 84–92 (2012).
- [13] H. Zhou, Y. Geng, W. Cui, S.-W. Huang, Q. Zhou, K. Qiu, and C. Wei Wong, "Soliton bursts and deterministic dissipative Kerr soliton generation in auxiliary-assisted microcavities," *Light Sci. Appl.* **8**, 50 (2019).
- [14] P. Marin-Palomo, J. N. Kemal, M. Karpov, A. Kordts, J. Pfeifle, M. H. P. Pfeifer, P. Trocha, S. Wolf, V. Brasch, M. H. Anderson, R. Rosenberger, K. Vijayan, W. Freude, T. J. Kippenberg, and C. Koos, "Microresonator-based solitons for massively parallel coherent optical communications," *Nature* **546**, 274–279 (2017).
- [15] F.-X. Wang, W. Wang, R. Niu, X. Wang, C.-L. Zou, C.-H. Dong, B. E. Little, S. T. Chu, H. Liu, P. Hao, S. Liu, S. Wang, Z.-Q. Yin, D.-Y. He, W. Zhang, W. Zhao, Z.-F. Han, G.-C. Guo, and W. Chen, "Quantum key distribution with on-chip dissipative Kerr soliton," *Laser Photonics Reviews*, (2019).
- [16] M.-G. Suh, K. J. Vahala, "Soliton microcomb range measurement," *Science* **359**, 884–887 (2018).
- [17] M.-G. Suh, Q.-F. Yang, K. Y. Yang, X. Yi, and K. J. Vahala, "Microresonator soliton dual-comb spectroscopy," *Science* **354**, 600–603 (2016).
- [18] A. Dutt, C. Joshi, X. Ji, J. Cardenas, Y. Okawachi, K. Luke, A. L. Gaeta, and M. Lipson, "On-chip dual-comb source for spectroscopy," *Science Advances* **4**, e1701858 (2018).
- [19] W. Weng, E. Lucas, G. Lihachev, V. E. Lobanov, H. Guo, M. L. Gorodetsky, and T. J. Kippenberg, "Spectral Purification of Microwave Signals with Disciplined Dissipative Kerr Solitons," *Phys. Rev. Lett.* **122**, 013902 (2019).
- [20] Z. L. Newman, V. Maurice, T. Drake, J. R. Stone, T. C. Briles, D. T. Spencer, C. Fredrick, Q. Li, D. Westly, B. Ilic, B. Shen, M.-G. Suh, K. Y. Yang, C. Johnson, D. M. S. Johnson, L. Hollberg, K. J. Vahala, K. Srinivasan, S. A. Diddams, J. Kitching, S. B. Papp, M. T. Hummon, "Architecture for the photonic integration of an optical atomic clock," *Optica* **6**, 680–685 (2019).
- [21] M.-G. Suh, X. Yi, Y.-H. Lai, S. Leifer, I. S. Grudin, G. Vasisht, E. C. Martin, M. P. Fitzgerald, G. Doppmann, J. Wang, D. Mawet, S. B. Papp, S. A. Diddams, C. Beichman, and K. Vahala, "Searching for exoplanets using a microresonator astrocomb," *Nature Photonics* **13**, 25–30 (2019).
- [22] E. Obrzud, M. Rainer, A. Harutyunyan, M. H. Anderson, J. Liu, M. Geiselmann, B. Chazelas, S. Kundermann, S. Lecomte, M. Cecconi, A. Ghedina, E. Molinari, F. Pepe, F. Wildi, F. Bouchy, T. J. Kippenberg, and T. Herr, "A microphotonic astrocomb," *Nature Photonics* **13**, 31–35 (2019).
- [23] F. Leo, L. Gelens, P. Emplit, M. Haelterman, and S. Coen, "Dynamics of one-dimensional Kerr cavity solitons," *Opt. Express* **21**, 9180–9191 (2013).
- [24] C. Bao, J. A. Jaramillo-Villegas, Y. Xuan, D. E. Leaird,

- M. Qi, A. M. Weiner, "Observation of Fermi-Pasta-Ulam Recurrence Induced by Breather Solitons in an Optical Microresonator," *Phys. Rev. Lett.* **117**, 163901 (2016).
- [25] M. Yu, J. K. Jang, Y. Okawachi, A. G. Grith, K. Luke, S. A. Miller, X. Ji, M. Lipson, and A. L. Gaeta, "Breather soliton dynamics in microresonators," *Nature communications* **8**, 14569 (2017).
- [26] E. Lucas, M. Karpov, H. Guo, M. Gorodetsky, T. J. Kippenberg, "Breathing dissipative solitons in optical microresonators," *Nature communications* **8**, 736 (2017).
- [27] H. Guo, E. Lucas, M. H. P. Pfeifer, M. Karpov, M. Anderson, J. Liu, M. Geiselmann, J. D. Jost, and T. J. Kippenberg, "Intermode Breather Solitons in Optical Microresonators," *Phys. Rev. X* **7**, 041055 (2017).
- [28] C. Bao, Y. Xuan, C. Wang, A. Fulop, D. E. Leaird, V. Torres-Company, M. Qi, A. M. Weiner, "Observation of Breathing Dark Pulses in Normal Dispersion Optical Microresonators," *Phys. Rev. Lett.* **121**, 257401 (2018).
- [29] K. Luke, A. Dutt, C. B. Poitras, M. Lipson, "Overcoming Si_3N_4 film stress limitations for high quality factor ring resonators," *Optics express* **21**, 22829–22833 (2013).
- [30] Y. K. Chembo, N. Yu, "Modal expansion approach to optical-frequency-comb generation with monolithic whispering-gallery-mode resonators," *Phys. Rev. A* **82**, 033801 (2010).
- [31] T. Hansson, D. Modotto, and S. Wabnitz, "On the numerical simulation of Kerr frequency combs using coupled mode equations," *Optics Communications*, **312**, 134–136 (2014).
- [32] X. Guo, C.-L. Zou, H. Jung, Z. Gong, A. Bruch, L. Jiang, H. X. Tang, "Efficient Generation of a Near-visible Frequency Comb via Cherenkov-like Radiation from a Kerr Microcomb," *Phys. Rev. Applied* **10**, 014012 (2018).
- [33] R. Niu, S. Wan, S.-M. Sun, T.-G. Ma, H.-J. Chen, W.-Q. Wang, Z.-Z. Lu, W.-F. Zhang, G.-C. Guo, C.-L. Zou, and C.-H. Dong, "Repetition rate tuning of soliton in microrod resonators," arXiv:1809.06490 (2018).
- [34] Y. Geng, X. Huang, W. Cui, Y. Ling, B. Xu, J. Zhang, X. Yi, B. Wu, S.-W. Huang, K. Qiu, C. W. Wong, H. Zhou, "Terabit optical OFDM superchannel transmission via coherent carriers of a hybrid chip-scale soliton frequency comb," *Opt. Lett.* **43**, 2406–2409 (2018).